Radiation Measurements 154 (2022) 106757

Contents lists available at ScienceDirect

Radiation Measurements

journal homepage: www.elsevier.com/locate/radmeas

Measurements of natural radiation with an MDU Liulin type device at ground and in the atmosphere at various conditions in the Arctic region

Alexander Mishev [a,b,*], Alexandros Binios [a], Esa Turunen [a], Ari-Pekka Leppänen [c], Nicholas Larsen [a], Eija Tanskanen [a], Ilya Usoskin [a,b], Jouni Envall [a], Toivo Iinatti [a], Pasi Lakkala [a]

[a] Sodankylä Geophysical Observatory, University of Oulu, Finland
[b] Space Physics and Astronomy Research Unit, University of Oulu, Finland
[c] Radiation and Nuclear Safety Authority - STUK, Rovaniemi, Finland

ARTICLE INFO

Keywords:
Galactic cosmic rays
Exposure to radiation
Scientific balloon flight
Precipitating particles
Stratosphere and troposphere

ABSTRACT

Measurements of the natural radiation background with different devices and at various conditions are important from a methodological point of view in order to compare and eventually inter-calibrate different experimental sets, also to provide a reliable basis for improving the existing models for assessment of the environmental radiation in the Earth's atmosphere. Here, we report results from methodological measurements with a small portable device, namely mobile dosimetry unit (MDU)-1 Liulin, performed in different conditions in the Arctic region, including the altitude profile of the atmospheric radiation obtained during the flight of the HEMERA-2 zero-pressure balloon. A comparison with a calibrated device is also performed. It was demonstrated that the MDU-1 Liulin can provide reliable measurements of the radiation background in the Arctic atmosphere during a zero-pressure balloon flight.

1. Introduction

Different populations of energetic precipitating particles (EPPs) enter the Earth's atmosphere, eventually leading to ionization of the ambient air (e.g. Mironova et al., 2015, and references therein). Solar UV, EUV, and X-ray radiation mostly determine the ion production in the upper atmosphere, whilst the precipitating energetic particles affect the stratospheric and tropospheric ionization. Below 100 km above sea level (asl), the atmospheric ionization is mostly due to the omnipresent quasi-constant slightly variable flux of galactic cosmic rays (GCRs), which can be sporadically enhanced by solar energetic particles (SEPs) and/or precipitating relativistic electrons (e.g. Mironova et al., 2015, and references therein).

When a high-energy particle enters the Earth's atmosphere, initiate a complicated nuclear-meson-electromagnetic (NME) cascade, via mostly hadron interactions. NME cascade is a particle shower produced by a series of consecutive interactions of the primary particle with the atmospheric constituents, yielding large amounts of secondaries. For instance when a primary cosmic proton and/or heavier nucleus interacts with an atmospheric constituent it produces essentially hadrons such as pions and kaons. Pions and kaons decay nearly instantly to other particles, e.g. neutral pions decay into two gammas, the latter producing electron–positron pairs giving rise of the electromagnetic component of the developing shower. The charged pions mostly decay into muons, giving rise of the muon component of the shower. We note, that secondaries, in their turn also interact with atmospheric constituents and produce other particles, feeding the development of the shower, until threshold energy for the production of new particles is reached (e.g. Gaisser et al., 2016).

The omnipresent flux of GCRs consists of (in the number of particles) mainly of protons (~90%) and α-particles (~8%), as well as a small amount of heavier nuclei, measured with a good precision by PAMELA (Payload for Antimatter Matter Exploration and Light-nuclei Astrophysics) (e.g. Adriani et al., 2017) and AMS-02 (Alpha Magnetic Spectrometer) space experiments (Aguilar et al., 2021). GGR flux is slightly modulated by the solar wind and reveals notable variations throughout the solar cycle (e.g. Potgieter, 2013, and references therein). Another, but occasional source of atmospheric ionization is due to SEPs, which are particles accelerated within and in the vicinity of the Sun during solar eruptive events, such as solar flares and coronal mass ejections (CMEs) (e.g. Klein and Dalla, 2017, and references therein). In addition, relativistic electrons can precipitate from the radiation belts and contribute to increased atmospheric ionization, accordingly radiation field (e.g. Artamonov et al., 2016; Mironova et al., 2019; Xu et al., 2021). In such a way, the EPPs determine the complex radiation field in the stratosphere and troposphere of the Earth (e.g. Spurny et al., 1996; Vainio et al., 2013).

* Corresponding author at: Space Physics and Astronomy Research Unit, University of Oulu, Finland.
E-mail addresses: alexander.mishev@oulu.fi, alex_mishev@yahoo.com (A. Mishev).

https://doi.org/10.1016/j.radmeas.2022.106757
Received 14 January 2022; Received in revised form 1 April 2022; Accepted 11 April 2022
Available online 20 April 2022

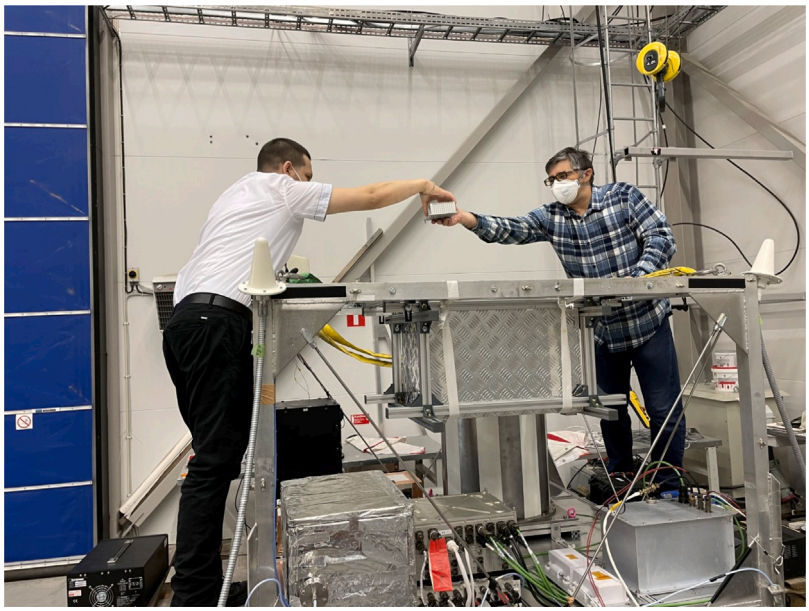

Fig. 1. Mounting of MDU-1 Liulin by two of the authors (A. Binios on the left, A. Mishev on the right) in the isolated box and the gondola of HEMERA mission. Photo by Esa Turunen.

Precipitating high-energy charged particles play an important role in the processes of the Earth's atmosphere, specifically in induced ionization and the corresponding influence on atmospheric physics and chemistry (e.g. Turunen et al., 2009; Mironova et al., 2015; Xu et al., 2018, and references therein). Therefore, a careful study of EPP fluxes as well as their terrestrial effects, particularly the radiation field in the atmosphere, is crucial for understanding the ionization processes and assessment of exposure to radiation for aircraft crew and passengers (e.g. Vainio et al., 2009, and references therein). The measurements of the natural radiation with different devices at various conditions are important for inter-calibration of different experiments and to provide a reliable basis to improve the existing models related to EPP terrestrial effects and the dosimetric models for exposure to radiation in the atmosphere.

In this article, we present preliminary results with all corresponding on-ground measurements of a MDU-1 Liulin during B-TRUE experiment flown on a HEMERA-2 scientific balloon flight on 11 September 2021, with the aim of measuring the altitude profile of secondary cosmic radiation in the Arctic atmosphere.

2. Materials and methods

Measurements of the complex radiation environment at aviation flight or greater altitudes are challenging, the latter being specifically in the stratosphere (e.g. Spurny et al., 1996). In fact, scientific balloon operation is very similar to space flight in many aspects, particularly the mass and dimensions of the payload (e.g. Ubertini, 2008). Over the years large diversity of instruments and methods employed for space radiation dosimetry have been developed (e.g. Caffrey and Hamby, 2011; Straume et al., 2016; Berger et al., 2017).

Active detectors, e.g. DOSTEL and/or Mobile Dosimetry Unit (MDU) Liulin, allow one to assess the absorbed dose in real-time. In this study, we employed the MDU-1 Liulin dosimetric instrument, based on a silicon semiconductor detector, the specifications are given in Appendix A. The device measures the deposited energy and the amount of interacting particles in the detector, providing the dose rate in silicon and particle flux, and it is widely used for measurements of the exposure to radiation (absorbed dose) in space missions, (for details see Dachev et al., 2011, 2015, and references therein). Besides, the Liulin type detectors were used and compared with other devices at jet flight and high-mountain altitudes, as well as models for assessment of the exposure to radiation in the atmosphere due to cosmic rays, and good agreement was reported (e.g. Mishev and Usoskin, 2015; Meier et al., 2016; Mishev, 2016). Here, the MDU-1 Liulin was flown under the HEMERA-2 zero-pressure scientific balloon project in the frame of B-TRUE (Balloon borne Telescope for Relativistic and Ultra-relativistic Electrons) experiment.

In general, different types of balloons are available for the community, depending on the mission type, e.g.,: zero-pressure balloons for heavy payloads and short to medium duration of about a day up to several days; sounding balloons for very light payloads, usually providing only ascent and descent to the stratosphere; super-pressure balloons for very long duration flights. Usually, the payloads can be flown at altitudes up to about 40 km. In contrast to satellite-borne missions, stratospheric balloons can be operated at relatively low cost. In addition, the balloon missions are for shorter duration compared to satellites, and in most cases, the payloads are recovered, upgraded if necessary, and readied to fly again (e.g. Mantovani and HEMERA Team, 2019). Therefore, for a mission aiming to register of secondary cosmic ray radiation and/or relativistic electrons precipitation, specifically the assessment of altitude profile of the complex radiation field due to EPP, zero-pressure stratospheric balloons are very suitable (long duration compared to sub-orbital rockets, lowers costs, recovery of the payload).

HEMERA represents a research infrastructure, encompassing different teams in the field of tropospheric and stratospheric balloon-borne research, including astrophysics, atmospheric physics and chemistry, climate research, biology, space research and technology (for details see Mantovani and HEMERA Team, 2019). On 11 of September 2021 a new stratospheric zero-pressure balloon launch was performed from the Esrange base of the Swedish Space Corporation, near to Kiruna in Northern Sweden. After a successful launch thanks to the Esrange team and favorable meteorological conditions, the flight lasted nine hours in total, floated for three hours in the stratosphere at the ceiling altitude of 33 km, details are given in Appendix C. The MDU-1 Liulin was launched in the B-TRUE experiment, which is a Finnish experiment aiming measurements of EPP, specifically relativistic electrons in the high Arctic atmosphere Figs. 1, 2.

Finally, in order to perform a preliminary and subsequent analysis of the derived results, we computed the cut-off rigidity at the launch site and the over-flown site in Finland, that is Rovaniemi, the latter

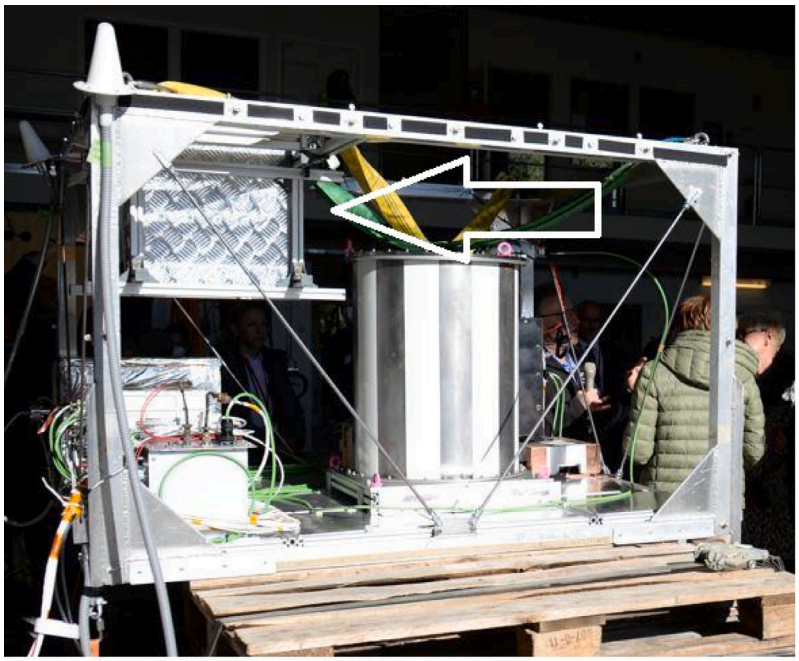

Fig. 2. The gondola of HEMERA scientific balloon with the MDU-1 Liulin mounted in the Al box. The arrow indicates the Al box with the MDU-1 Liulin inside. Photo provided by David Hagsved.

located about 300 km south-east of Kiruna. Here the cut-off rigidity was computed with a newly developed tool by the authors, which details will be presented in forthcoming work, as well as with the MAGNETOCOSMICS code, explicitly considering the measured K_p index corresponding to the exact period of the launch (Desorgher et al., 2005). In both models, during the computations, a combination of the IGRF geomagnetic model as the internal field (Thébault et al., 2015) and the Tsyganenko 89 model as the external field (Tsyganenko, 1989) were employed allowing straightforward computations (Kudela and Usoskin, 2004; Kudela et al., 2008; Nevalainen et al., 2013). The cut-off rigidity computed with the MAGNETOCOSMICS code was R_c = 0.449 GV and R_c = 0.566 GV, for the Esrange Kiruna and Rovaniemi, respectively. Slightly greater effective cut-offs were obtained employing a new magnetospheric tool, developed in Sodankylä Geophysical Observatory (SGO), the details will be given in forthcoming work, namely about R_c = 0.417–0.513 GV and R_c=0.562–0.646 GV, for the Esrange Kiruna and for Rovaniemi, respectively, the largest difference obtained assuming the magnetopause model of Sibeck (ellipsoid magnetopause model) (e.g. Zong et al., 2020, and references therein). Here we would like to stress that for the computation of absorbed dose due to GCRs, accordingly data analysis of the HEMERA-2 mission, this difference is not important (Copeland et al., 2008; Mishev et al., 2021). The computed cut-off rigidities allowed us to quantify the measurements in comparison with a model for assessment of the exposure to radiation (i.e. absorbed dose) in the atmosphere (see Section 3).

3. Results

First, we present the results from several methodological measurements, which are important for planning similar experiment(s), as well as the B-TRUE mission itself. It is important to ensure an appropriate temperature environment of the device, since the temperature can drop to about −60 °C in the stratosphere, while the operating regime of MDU-1 Liulin is from −20 to about +40 °C (Dachev et al., 2015). For this purpose a thermally insulated aluminum box as depicted in Figs. 1, 2 was constructed, using a standard aluminum one with 20 cm styrofoam insulation shown in Fig. 3, details are given in the Appendix C.

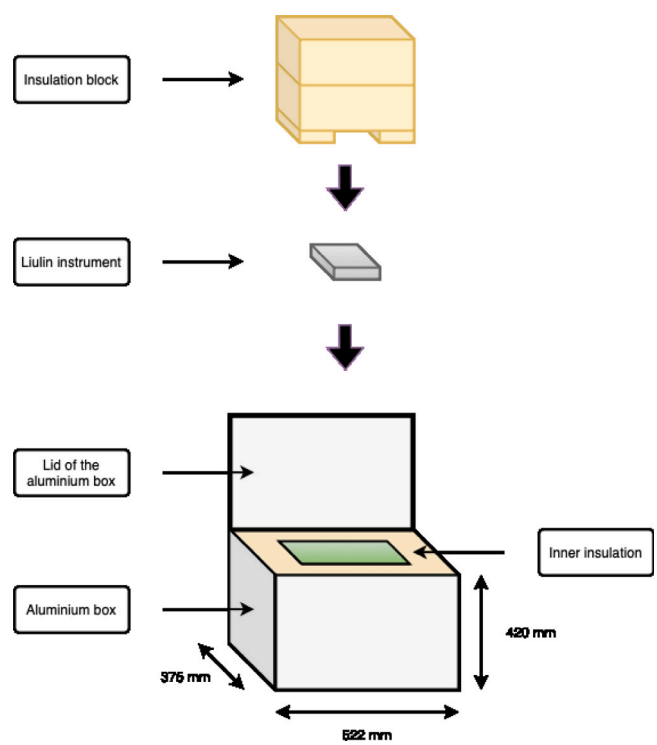

Fig. 3. Sketch of the MDU-1 Liulin payload at HEMERA mission.

We performed several measurements of the natural radiation background, that is outside of SGO facility with MDU-1 Liulin inside and outside of the transportation box, respectively, as well as on site at Esrange Kiruna in the insulated box, summarized in Table 1. In addition, a comparative measurement with a calibrated Rados RDS-200 dosimeter, the specifications are given in Appendix B, and MDU-1 Liulin, of an increased radiation field was carried out. The radiation source we used

Table 1
Summary of the measurements performed with MDU-1 Liulin at different conditions. Measurements 1–2 and 6 are performed with MDU-1 Liulin in the transportation box, while 3 in conditions similar to the flight conditions. The data from measurement 4 are given in ambient dose equivalent in order to compare with the calibrated device in STUK. The measurements 5 and 7 are performed at ground as flight simulation i.e., in the insulated box, where 5 is in the cold camera Fig. 5. The standard deviation of the measurements SD is given in column 6.

Series	Site	Time	Integration time [min]	Abs. dose [μGy/h]	SD [μGy/h]
1	SGO inside	17.08.2021	720	0.0994	0.027
2	SGO outside	17.08.2021	150	0.0918	0.023
3	SGO outside	17.08.2021	120	0.0992	0.029
4	Rovaniemi inside	18.08.2021	90	18.6	1.03
5	Kemi cold test	31.08.2021	120	0.0969	0.049
6	SGO-Kiruna on the road	04.09.2021	380	0.0954	0.03
7	Esrange Kiruna in the gondola	06–07.09.2021	840	0.09	0.02

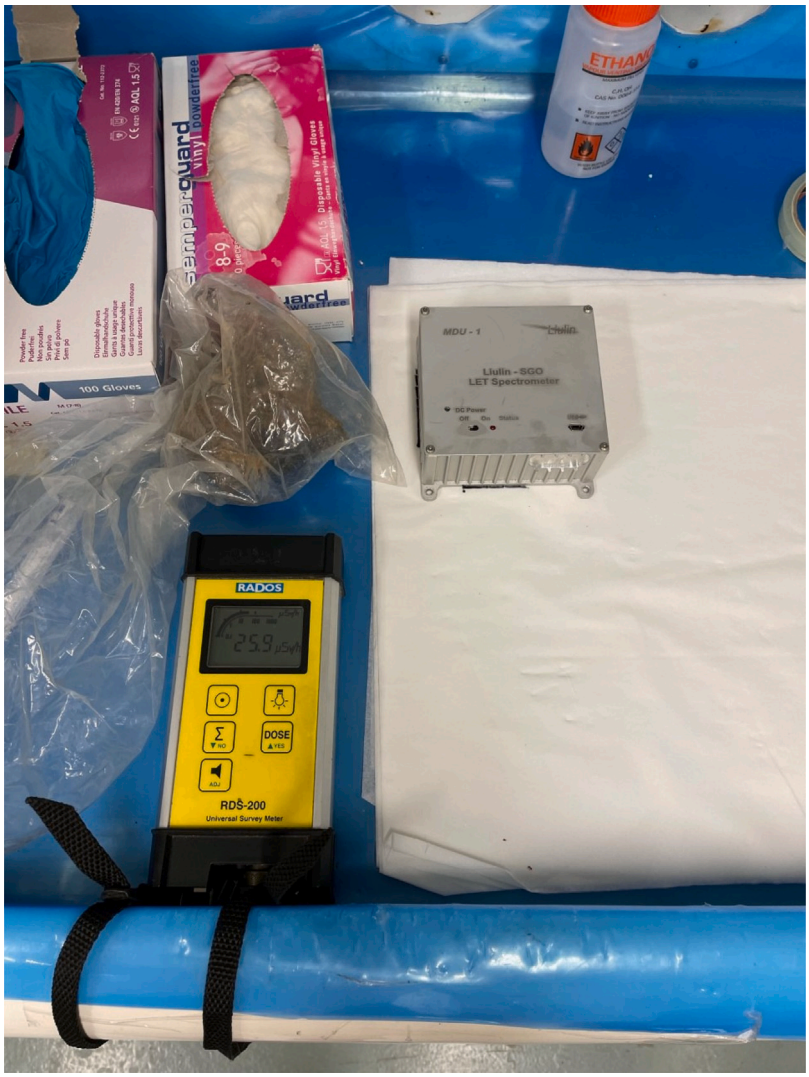

Fig. 4. MDU-1 Liulin and Rados RDS-200 comparative measurements at STUK Rovaniemi laboratory. The MDU-1 Liulin detector is on the right and Rados RDS-200 at the bottom and the rock containing natural uranium in the middle in a plastic bag.

was a rock containing elevated concentrations of natural uranium and its daughters. The test was performed at STUK's facility in Rovaniemi, Finland. The aim was to check the behavior of the MDU-1 Liulin in increased compared to the background radiation field, yet different to that during a scientific balloon flight as interacting particles and energy range, see Fig. 4 and Table 1. The measurements 1–3 described in Table 1 were performed in wet cloudy weather, but without rain conditions, outside of SGO technical facility. Measurement 4 was performed in the ground floor of STUK facility in Rovaniemi, with light rainy conditions outside. Note, that the calibrated Rados RDS-200 dosimeter measured slightly greater values, mostly due to the different sensitivity and geometry of the experiment, yet a satisfactory result was achieved.

A flight simulation measurement was performed of SGO HEMERA-2 Payload, consisting of the MDU-1 Liulin, placed inside the thermally insulated aluminum box, at the Electronics Test Laboratory of Lapland University of Applied Sciences in Kemi, Finland (Fig. 5). The payload was kept for about 2 h in a cold chamber, which was set to temperature of −50.0 °C, corresponding to the temperature during the flight, that is the temperature in the cold chamber was selected in order to simulate the worst flight conditions at 35 km altitude. Note, that air pressure in

Fig. 5. The SGO HEMERA-2 Payload, consisting of MDU-1 Liulin inside the thermally insulated aluminum box e.g. in flight configuration in the Espec EGNX12-6CWL test chamber (380 l) at the Electronics Test Laboratory of Lapland University of Applied Sciences in Kemi, Finland. Photo by Esa Turunen.

the chamber was not changed. Instead the pressure was stable at the ground level pressure 1030 mb. The payload temperature, that is the insulated box, cooled from 20.6 °C to 0.0 °C in exactly 2 h. Thereafter the chamber was slowly heated back to +25 °C, while the payload continued cooling down, with minimum temperature of −4.3 °C 30 min after starting the heating cycle. The results from this measurement (5) is given in Table 1. Note, that the radiation background outside of the cold chamber is similar to that in SGO facility and Rovaniemi.

Measurement 6 was performed on the road between SGO and Kiruna, the device being in the transportation box in a wagon car trunk. The measurements in Esrange were performed inside the assembly dome of the facility.

One can see that the MDU-1 Liulin provided reliable data of the radiation background on site, both at SGO and Kiruna. Moreover, similar test measurements have been performed during the transportation of the device from SGO to Kiruna, shown in Table 1. Here we would like to point out that the MDU-1 Liulin in general is very sensitive to vibrations, yet such effect was not observed during the trip. Therefore, the construction of the box provides a basis for reliable good quality measurements in flight conditions (low outside temperature, vibrations). From those series of measurements, we can conclude that the MDU-1 Liulin is a relatively precise device, and most importantly the insulated box provides the necessary temperature conditions for the device to operate properly in the stratosphere. Here we emphasize, that the radiation field at flight altitude(s) differs from the surface background radiation, specifically the energy and type of the particles(radiation). Therefore, more detailed studies of the impact of the insulated box on the MDU-1 measurements are necessary, which is beyond the topic of present paper.

Finally, here we present the altitude profile of the exposure to radiation (i.e. absorbed dose) in the atmosphere obtained with MDU-1 Liulin during the HEMERA-2 zero-pressure scientific balloon flight on 11 September 2021 see Fig. 6. In this case the payload consisted of the MDU-1 Liulin was placed inside the thermally insulated aluminum box. Here, we present both the raw data as well as the 10 min. running mean. The preliminary analysis shows good agreement with Oulu model for assessment of the exposure to radiation (i.e. absorbed dose) at flight altitudes as well as with similar measurements (for details see Wissmann et al., 2013; Mishev and Usoskin, 2015), the full details of the analysis is planned as forthcoming work. Yet we present a comparison with recent models, for details see Table 2. Here we selected all the available measurements at the given altitude and computed the mean absorbed dose with the corresponding standard deviation(s). We emphasize, that the relatively fast balloon ascend in the low atmosphere resulted in significant deviation(s), specifically at 3 km.

Here, the comparison of the measurements is performed with the Oulu models for exposure to radiation (i.e. absorbed dose) (Mishev

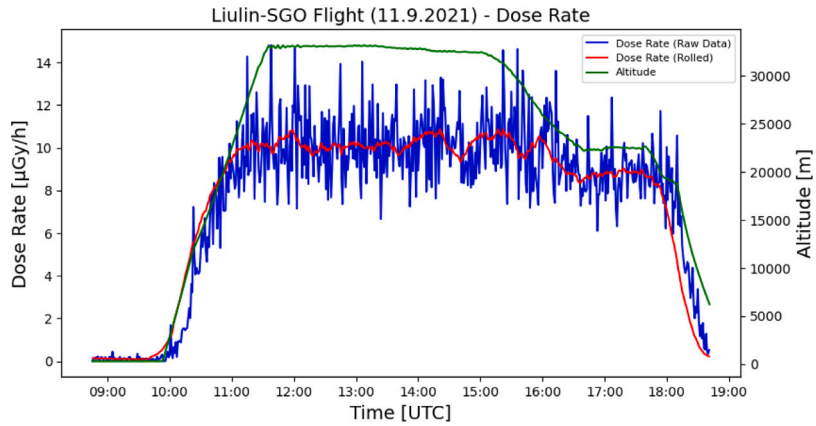

Fig. 6. Altitude profile of the absorbed dose measured with MDU-1 Liulin — raw data and 10 min running mean as depicted in the legend.

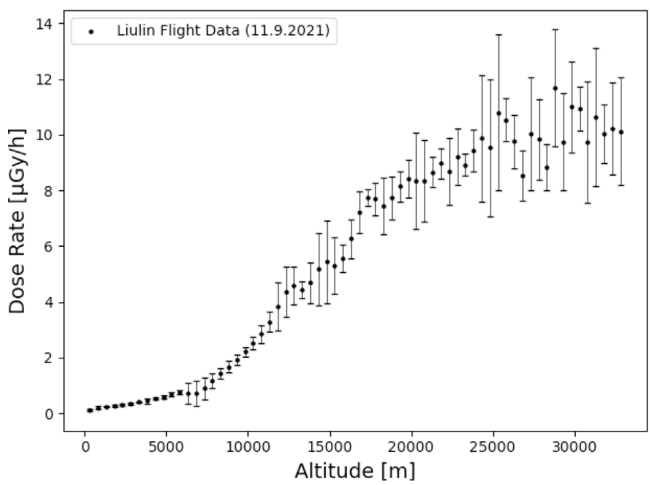

Fig. 7. Processed absorbed dose vs. altitude measured with MDU-1 Liulin.

Table 2
Comparison between MDU-1 Liulin measurements with Oulu dosimetric and atmospheric ionization models. Column 1–2 correspond to the altitude in km and kft, respectively. Column 3 correspond to MDU-1 Liulin measurement, column 4 to the modeled absorbed dose, while columns 5–6 to ion production in air.

Alt. [km]	Alt. [kft]	Dose rate [μGy/h]		Ionization [ion pairs/s cm^3]	
		Liulin	Model	Liulin	Model
3	9.85	0.37 ± 0.9	0.22 ± 0.08	16 ± 6	21 ± 5
10.7	35	2.8 ± 0.7	6.4 ± 2.0	43 ± 14	55 ± 12
15.2	50	5.2 ± 1.3	7.7 ± 2.1	57 ± 18	62 ± 14

and Usoskin, 2015) and atmospheric ionization (Usoskin and Kovaltsov, 2006). The dose is computed similarly to Mishev and Hristova (2012), while the atmospheric ionization is obtained by straightforward conversion of the absorbed dose to deposited energy, explicitly considering the energy necessary for the production of one ion pair, that is 35 eV according to Porter et al. (1976), namely by conversion of the absorbed dose [J/kg] to [eV/kg], and subsequently to ion pairs. For the GCR spectrum, we assumed the force field model (Gleeson and Axford, 1968; Caballero-Lopez and Moraal, 2004), considering the local interstellar spectrum by Vos and Potgieter (2015) and the modulation potential computed as in Usoskin et al. (2011). The modeled ion production rate is computed similarly to Mishev and Velinov (2020) and Pätsi and Mishev (2022) employing the NRLMSISE-00 atmospheric model by Picone et al. (2002).

One can see the very good agreement between measured and modeled ion production rates in the atmosphere (columns 5–6 of Table 2), whilst the difference in the absorbed dose can be attributed to the contribution of the natural radiation background in the measurements at an altitude of 3 km and the limited sensitivity of the MDU-1 Liulin to secondary hadrons at greater altitudes, yet more detailed analysis is necessary, which is beyond the scope of this study.

An apparent spike in the raw data is observed, which corresponds to the time of landing, that is the hit of the gondola to the ground. Since the device is very sensitive to vibrations, this spike is due to the hit of the balloon gondola (the payload) with the ground, which will not be considered in future data analysis. Note, that similarly to some previous measurements (e.g. Fig. 3 in Wissmann et al., 2013; Hands et al., 2016), the Regener–Pfotzer maximum (Regener and Pfotzer, 1935) in absorbed dose is barely seen (Fig. 7), most-likely due to high-latitude-low-rigidity cut-off location of the experiment leading to dominant low-energy contribution of the GCRs, as well as the relatively fast balloon ascend. However, a further more detailed analysis is necessary, which is beyond the scope of this study.

4. Summary

Here, we reported results of measurements of the natural radiation with an MDU-1 Liulin type device at various conditions, specifically in the Arctic region, namely at ground (indoor and outdoor) at SGO site, the cold test, i.e. the behavior of the device inside an insulated with styrofoam box in cold temperature room and in zero-pressure scientific balloon flight. All measurements were performed with 1-min time resolution and with different integration over the corresponding experiment. It was shown that the isolated Al box provides the necessary temperature regime, without affecting the MDU-1 Liulin performance, therefore can be used for similar future missions, including flight(s) with the same instrument. Considering the quality of the obtained data, one can see that MDU-1 Liulin is a useful device for the measurements of the complex radiation field in the troposphere and stratosphere, including the Arctic or Antarctic region, where is a lack of systematic studies. The obtained data are useful to deepen our understanding of aviation dosimetry, atmospheric and space physics by providing the necessary basic knowledge of the employment of returnable payload which can measure the radiation in the atmosphere due to different populations of precipitating energetic particles.

Additionally, we are looking for opportunities with scientific balloon flights and high-altitude platform systems for further studies with the prepared instrument consisting of the MDU-1 Liulin, thermometers, and their protective casing.

Declaration of competing interest

The authors declare that they have no known competing financial interests or personal relationships that could have appeared to influence the work reported in this paper.

Acknowledgments

The HEMERA balloon program is supported under Horizon 2020 framework Program of the European Union under the grant 730970. This work was supported by the Academy of Finland (projects 330064 QUASARE, 321882 ESPERA). We warmly acknowledge the Esrange team lead by David Hagsved and all colleagues from other experiments for fruitful discussion. We warmly acknowledge Mika Mört, Soile Sääski from the Electronics Test Laboratory of Lapland University of Applied Sciences in Kemi, Finlad. We also acknowledge prof. T. Dachev from Institute for Space Physics and Technology of Bulgarian Academy of Sciences for the technical support and scientific advise.

Appendix A. MDU-1 Lulin specifications

Here we present several specification, according to the provided by the manufacturer manual, of MDU-1 Luilin used for the HEMERA zero-pressure balloon flight on 11 September 2021. The main measurement unit in the spectrometer is the amplitude of the pulse after the preamplifier from charged particles and/or gamma quanta. The pulse is proportional by a factor of 240 mV/MeV to the energy loss in the detector, accordingly to the dose. A 12-bit analog to digital converter digitizes the amplitudes in a 256-channels spectrum.

- Dose range: 0.093 nGy–1.56 mGy;
- Flux range: - 0.01–1250 part/cm^2 s;
- Pulse height analysis range: - 9.25 mV–5.0 V;
- Temperature range: −20 °C – +40 °C;
- Battery type: Lithium 3.6 V 2 pieces;
- Size (including batteries): 110 × 100 × 45 mm;
- Total mass (including batteries): 0.57 kg;
- Surface of the Silicon detector: 2 cm^2;
- The Si is behind: 0.3 mm aluminum + 1 mm air + 0.06 mm copper + 0.2 mm plastic shielding;

Appendix B. Rados RDS-200 specifications

The comparative measurement of MDU-1 Lulin with calibrated device was performed in STUK Rovaniemi. Here, we provide some technical details about the used device, that is Rados RDS-200. According to the manufacturer:

Type of detector

Rados RDS-200, detector consists of two energy compensated GM-tubes;

Manufacturer: Rados Technologies Oy, Turku, Finland;

Range: 0.01 μSv/h–10 Sv/h;

Radiation detected: gamma and X-rays, 50 keV...1.3 MeV;

Date of calibration: 29 January 2019 in STUK's accredited dosimetry laboratory.

Calibration accuracy: ± 5%, ^{137}Cs;

Details are given in http://www.inspection-kits.com/RDS-200-Universal-Survey-Meter-s-500-604.html. We emphasize that the instrument can detect also high-energy secondary cosmic rays, but it is not calibrated in terms of dose rates at energies above about 1.3 MeV, therefore the calibration tends to get poor (uncertainty greater than 30%) when the energies are greater than 3 MeV.

Appendix C. Payload and balloon flight specifications

The MDU-1 Lulin was flown in the HEMERA zero-pressure balloon mounted in a gondola. The span of the Gondola was 1.5 × 1.5 × 1 m. The total mass of the Gondola was 336 kg, of which 90 kg for the gondola frame and 21 kg for E-link including batteries and cabling. An Airstar 150 Z balloon with volume of 150 000 m^3 filled with Helium was used. The balloon was released at 09:53 UTC on 11 September 2021. The balloon ascended till 11:35 UTC and reached an apogee of 33.14 km and then kept a stable float at around 33 km for 3 h 25 m.

We used an aluminum box with added insulation for housing the payload.

Inner dimensions:

length 500 mm; width 350 mm; depth 400 mm;

Outer dimensions of the box:

length 522 mm; width 375 mm; depth 420 mm;

The aluminum is 3 mm thick.

For insulation we used Finnfoam F-700 styrofoam, with density of 40 kg/m^3.

References

Adriani, O., Barbarino, G.C., Bazilevskaya, G.A., Bellotti, R., Boezio, M., Bogomolov, E.A., Bongi, M., Bonvicini, V., Bottai, S., Bruno, A., Cafagna, F., Campana, D., Carlson, P., Casolino, M., Castellini, G., De Santis, C., Di Felice, V., Galper, A.M., Karelin, A.V., Koldashov, S.V., Koldobskiy, S., Krutkov, S.Y., Kvashnin, A.N., Leonov, A., Malakhov, V., Marcelli, L., Martucci, M., Mayorov, A.G., Menn, W., Mergè, M., Mikhailov, V.V., Mocchiutti, E., Monaco, A., Munini, R., Mori, N., Osteria, G., Panico, B., Papini, P., Pearce, M., Picozza, P., Ricci, M., Ricciarini, S.B., Simon, M., Sparvoli, R., Spillantini, P., Stozhkov, Y.I., Vacchi, A., Vannuccini, E., Vasilyev, G., Voronov, S.A., Yurkin, Y.T., Zampa, G., Zampa, N., 2017. Ten years of PAMELA in space. Riv. Nuovo Cimento 40, 473–522. http://dx.doi.org/10.1393/ncr/i2017-10140-x.

Aguilar, M., Ali Cavasonza, L., Ambrosi, G., Arruda, L., Attig, N., Barao, F., Barrin, L., Bartoloni, A., Başeğmez-du Pree, S., Bates, J., Battiston, R., Behlmann, M., Beischer, B., Berdugo, J., Bertucci, B., Bindi, V., de Boer, W., Bollweg, K., Borgia, B., Boschini, M., Bourquin, M., Bueno, E., Burger, J., Burger, W., Burmeister, S., Cai, X., Capell, M., Casaus, J., Castellini, G., Cervelli, F., Chang, Y., Chen, G., Chen, H., Chen, Y., Cheng, L., Chou, H., Chouridou, S., Choutko, V., Chung, C., Clark, C., Coignet, G., Consolandi, C., Contin, A., Corti, C., Cui, Z., Dadzie, K., Dai, Y., Delgado, C., Della Torre, S., Demirköz, M., Derome, L., Di Falco, S., Di Felice, V., Díaz, C., Dimiccoli, F., von Doetinchem, P., Dong, F., Donnini, F., Duranti, M., Egorov, A., Eline, A., Feng, J., Fiandrini, E., Fisher, P., Formato, V., Freeman, C., Galaktionov, Y., Gámez, C., García-López, R., Gargiulo, C., Gast, H., Gebauer, I., Gervasi, M., Giovacchini, F., Gómez-Coral, D., Gong, J., Goy, C., Grabski, V., Grandi, D., Graziani, M., Guo, K., Haino, S., Han, K., Hashmani, R., He, Z., Heber, B., Hsieh, T., Hu, J., Huang, Z., Hungerford, W., Incagli, M., Jang, W., Jia, Y., Jinchi, H., Kanishev, K., Khiali, B., Kim, G., Kirn, T., Konyushikhin, M., Kounina, O., Kounine, A., Koutsenko, V., Kuhlman, A., Kulemzin, A., La Vacca, G., Laudi, E., Laurenti, G., Lazzizzera, I., Lebedev, A., Lee, H., Lee, S., Leluc, C., Li, J., Li, M., Li, Q., Li, S., Li, T., Li, Z., Light, C., Lin, C., Lippert, T., Liu, Z., Lu, S., Lu, Y., Luebelsmeyer, K., Luo, J., Lyu, S., Machate, F., Mañá, C., Marín, J., Marquardt, J., Martin, T., Martínez, G., Masi, N., Maurin, D., Menchaca-Rocha, A., Meng, Q., Mo, D., Molero, M., Mott, P., Mussolin, L., Ni, J., Nikonov, N., Nozzoli, F., Oliva, A., Orcinha, M., Palermo, M., Palmonari, F., Paniccia, M., Pashnin, A., Pauluzzi, M., Pensotti, S., Phan, H., Plyaskin, V., Pohl, M., Porter, S., Qi, X., Qin, X., Qu, Z., Quadrani, L., Rancoita, P., Rapin, D., Reina Conde, A., Rosier-Lees, S., Rozhkov, A., Rozza, D., Sagdeev, R., Schael, S., Schmidt, S., Schulz von Dratzig, A., Schwering, G., Seo, E., Shan, B., Shi, J., Siedenburg, T., Solano, C., Song, J., Sonnabend, R., Sun, Q., Sun, Z., Tacconi, M., Tang, X., Tang, Z., Tian, J., Ting, S.C., Ting, S., Tomassetti, N., Torsti, J., Tüysüz, C., Urban, T., Usoskin, I., Vagelli, V., Vainio, R., Valente, E., Valtonen, E., Vázquez Acosta, M., Vecchi, M., Velasco, M., Vialle, J., Wang, L., Wang, N., Wang, Q., Wang, S., Wang, X., Wang, Z., Wei, J., Weng, Z., Wu, H., Xiong, R., Xu, W., Yan, Q., Yang, Y., Yi, H., Yu, Y., Yu, Z., Zannoni, M., Zhang, C., Zhang, F., Zhang, F., Zhang, J., Zhang, Z., Zhao, F., Zheng, Z., Zhuang, H., Zhukov, V., Zichichi, A., Zimmermann, N., Zuccon, P., 2021. The alpha magnetic spectrometer (AMS) on the international space station: Part II results from the first seven years. Phys. Rep. 894, 1–116. http://dx.doi.org/10.1016/j.physrep.2020.09.003.

Artamonov, A., Mishev, A., Usoskin, I., 2016. Model CRAC:EPII for atmospheric ionization due to precipitating electrons: Yield function and applications. J. Geophys. Res. A 121, 1736–1743.

Berger, T., Burmeister, S., Matthia, D., Przybyla, B., Reitz, G., Bilski, P., Hajek, M., Sihver, L., Szabo, J., Ambrozova, I., Vanhavere, F., Gaza, R., Semones, E., Yukihara, E., Benton, E., Uchihori, Y., Kodaira, S., Kitamura, H., Boehme, M., 2017. Dosis & dosis 3d: Radiation measurements with the dostel instruments onboard the columbus laboratory of the iss in the years 2009–2016. J. Space Weather Space Clim 7.

Caballero-Lopez, R., Moraal, H., 2004. Limitations of the force field equation to describe cosmic ray modulation. J. Geophys. Res. 109, A01101.

Caffrey, J., Hamby, D., 2011. A review of instruments and methods for dosimetry in space. Adv. Space Res. 47, 563–574. http://dx.doi.org/10.1016/j.asr.2010.10.005.

Copeland, K., Sauer, H., Duke, F., Friedberg, W., 2008. Cosmic radiation exposure of aircraft occupants on simulated high-latitude flights during solar proton events from 1 January 1986 through 1 January 2008. Adv. Space Res. 42, 1008–1029. http://dx.doi.org/10.1016/j.asr.2008.03.001.

Dachev, T., Dimitrov, P., Tomov, B., Matviichuk, Y., Spurny, F., Ploc, O., Brabcova, K., Jadrnickova, I., 2011. Liulin type spectrometry dosimetry instruments. Radiat. Prot. Dosim. 144, 675–679. http://dx.doi.org/10.1093/rpd/ncq506.

Dachev, T., Semkova, J., Tomov, B., Matviichuk, Y., Dimitrov, P., Koleva, R., Malchev, S., Bankov, N., Shurshakov, V., Benghin, V., Yarmanova, E., Ivanova, O., Häder, D.P., Lebert, M., Schuster, M., Reitz, G., Horneck, G., Uchihori, Y., Kitamura, H., Ploc, O., Cubancak, J., Nikolaev, I., 2015. Overview of the liulin type instruments for space radiation measurement and their scientific results. Life Sci. Space Res. 4, 92–114. http://dx.doi.org/10.1016/j.lssr.2015.01.005.

Desorgher, L., Flückiger, E., Gurtner, M., Moser, M., Bütikofer, R., 2005. A geant 4 code for computing the interaction of cosmic rays with the earth's atmosphere. Internat. J. Modern Phys. A 20, 6802–6804.

Gaisser, T., Engel, R., Resconi, E., 2016. Cosmic Rays and Particle Physics. Cambridge University Press, Cambridge, UK.

Gleeson, L., Axford, W., 1968. Solar modulation of galactic cosmic rays. Astrophys. J. 154, 1011–1026.

Hands, A.D.P., Ryden, K.A., Mertens, C.J., 2016. The disappearance of the pfotzer-regener maximum in dose equivalent measurements in the stratosphere. Space Weather 14, 776–785. http://dx.doi.org/10.1002/2016SW001402.

Klein, K.L., Dalla, S., 2017. Acceleration and propagation of solar energetic particles. Space Sci. Rev. 212, 1107–1136. http://dx.doi.org/10.1007/s11214-017-0382-4.

Kudela, K., Bučik, R., Bobik, P., 2008. On transmissivity of low energy cosmic rays in disturbed magnetosphere. Adv. Space Res. 42, 1300–1306.

Kudela, K., Usoskin, I., 2004. On magnetospheric transmissivity of cosmic rays. Czech. J. Phys. 54, 239–254.

Mantovani, G., HEMERA Team, 2019. HEMERA: new science opportunities using tropospheric and stratospheric balloons. Mem. S. A. It. 90, 132.

Meier, M., Trompier, F., Ambrozova, I., Kubancak, J., Matthiä, D., Ploc, O., Santen, N., Wirtz, M., 2016. Concord: Comparison of cosmic radiation detectors in the radiation field at aviation altitudes. J. Space Weather Space Clim. 6. http://dx.doi.org/10.1051/swsc/2016017.

Mironova, I., Aplin, K., Arnold, F., Bazilevskaya, G., Harrison, R., Krivolutsky, A., Nicoll, K., Rozanov, E., Turunen, E., Usoskin, I., 2015. Energetic particle influence on the earth's atmosphere. Space Sci. Rev. 96.

Mironova, I., Artamonov, A., Bazilevskaya, G., Rozanov, E., Kovaltsov, G., Makhmutov, V., Mishev, A., Karagodin, A., 2019. Ionization of the polar atmosphere by energetic electron precipitation retrieved from balloon measurements. Geophys. Res. Lett. 46, 990–996. http://dx.doi.org/10.1029/2018GL079421.

Mishev, A., 2016. Contribution of cosmic ray particles to radiation environment at high mountain altitude: Comparison of Monte Carlo simulations with experimental data. J. Environ. Radioact. 153, 15–22. http://dx.doi.org/10.1016/j.jenvrad.2015.12.002.

Mishev, A., Hristova, E., 2012. Recent gamma background measurements at high mountain altitude. J. Environ. Radioact. 113, 77–82.

Mishev, A., Koldobskiy, S., Usoskin, I., Kocharov, L., Kovaltsov, G., 2021. Application of the verified neutron monitor yield function for an extended analysis of the GLE # 71 on 17 May 2012. Space Weather 19, e2020SW002626. http://dx.doi.org/10.1029/2020SW002626.

Mishev, A., Usoskin, I., 2015. Numerical model for computation of effective and ambient dose equivalent at flight altitudes: Application for dose assessment during gles. J. Space Weather Space Clim. 5, A10. http://dx.doi.org/10.1051/swsc/2015011.

Mishev, A., Velinov, P., 2020. Ionization effect in the earth's atmosphere during the sequence of October–November 2003 Halloween GLE events. J. Atmos. Sol.-Terr. Phys. 211, 105484. http://dx.doi.org/10.1016/j.jastp.2020.105484.

Nevalainen, J., Usoskin, I., Mishev, A., 2013. Eccentric dipole approximation of the geomagnetic field: Application to cosmic ray computations. Adv. Space Res. 52, 22–29.

Pätsi, S., Mishev, A., 2022. Ionization effect in the earth's atmosphere due to cosmic rays during the gle # 71 on 17 may 2012. Adv. Space Res. 69, 2893–2901. http://dx.doi.org/10.1016/j.asr.2022.02.008.

Picone, J., Hedin, A., Drob, D., Aikin, A., 2002. Nrlmsise-00 empirical model of the atmosphere: Statistical comparisons and scientific issues. J. Geophys. Res. Space Phys. 107, 1468.

Porter, H., Jackman, C., Green, A., 1976. Efficiencies for production of atomic nitrogen and oxygen by relativistic proton impact in air. J. Chem. Phys. 65, 154–167.

Potgieter, M., 2013. Solar modulation of cosmic rays. Living Rev. Sol. Phys. 10, 3. http://dx.doi.org/10.12942/lrsp-2013-3, URL: http://link.springer.com/10.12942/lrsp-2013-3.

Regener, E., Pfotzer, G., 1935. Vertical intensity of cosmic rays by threefold coincidences in the stratosphere. Nature 136, 718–719.

Spurny, F., Votockova, I., Bottollier-Depois, J., 1996. Geographical influence on the radiation exposure of an aircrew on board a subsonic aircraft. Radioprotection 31, 275–280.

Straume, T., Mertens, C., Lusby, T., Gersey, B., Tobiska, W., Norman, R., Gronoff, G., Hands, A., 2016. Ground-based evaluation of dosimeters for nasa high-altitude balloon flight. Space Weather 14, 1011–1025. http://dx.doi.org/10.1002/2016SW001406.

Thébault, E., Finlay, C.C., Beggan, C.D., Alken, P., Aubert, J., Barrois, O., Bertrand, F., Bondar, T., Boness, A., Brocco, L., Canet, E., Chambodut, A., Chulliat, A., Coïsson, P., Civet, F., Du, A., Fournier, A., Fratter, I., Gillet, N., Hamilton, B., Hamoudi, M., Hulot, G., Jager, T., Korte, M., Kuang, W., Lalanne, X., Langlais, B., Léger, J.M., Lesur, V., Lowes, F.J., Macmillan, S., Mandea, M., Manoj, C., Maus, S., Olsen, N., Petrov, V., Ridley, V., Rother, M., Sabaka, T.J., Saturnino, D., Schachtschneider, R., Sirol, O., Tangborn, A., Thomson, A., Tøffner-Clausen, L., Vigneron, P., Wardinski, I., Zvereva, T., 2015. International geomagnetic reference field: the 12th generation. Earth Planets Space 67, 79. http://dx.doi.org/10.1186/s40623-015-0228-9.

Tsyganenko, N., 1989. A magnetospheric magnetic field model with a warped tail current sheet. Planet. Space Sci. 37, 5–20.

Turunen, E., Verronen, P., Seppälä, A., Rodger, C., Clilverd, M., Tamminen, J., Enell, C.F., Ulich, T., 2009. Impact of different energies of precipitating particles on nox generation in the middle and upper atmosphere during geomagnetic storms. J. Atmos. Sol.-Terr. Phys. 71, 1176–1189.

Ubertini, P., 2008. Scientific balloons: historical remarks. Mem. Soc. Astr. It 79, 783.

Usoskin, I., Bazilevskaya, G., Kovaltsov, G., 2011. Solar modulation parameter for cosmic rays since 1936 reconstructed from ground-based neutron monitors and ionization chambers. J. Geophys. Res. 116, A02104.

Usoskin, I., Kovaltsov, G., 2006. Cosmic ray induced ionization in the atmosphere: Full modeling and practical applications. J. Geophys. Res. 111.

Vainio, R., Desorgher, L., Heynderickx, D., Storini, M., Flückiger, E., Horne, R., Kovaltsov, G., Kudela, K., Laurenza, M., McKenna-Lawlor, S., Rothkaehl, H., Usoskin, I., 2009. Dynamics of the earth's particle radiation environment. Space Sci. Rev. 147, 187–231.

Vainio, R., Valtonen, E., Heber, B., Malandraki, O., Papaioannou, A., Klein, K.L., Afanasiev, A., Agueda, N., Aurass, H., Battarbee, M., Braune, S., Dröge, W., Ganse, U., Hamadache, C., Heynderickx, D., Huttunen-Heikinmaa, K., Kiener, J., Kilian, P., Kopp, A., Kouloumvakos, A., Maisala, S., Mishev, A., Miteva, R., Nindos, A., Oittinen, T., Raukunen, O., Riihonen, E., Rodríguez-Gasén, R., Saloniemi, O., Sanahuja, B., Scherer, R., Spanier, F., Tatischeff, V., Tziotziou, K., Usoskin, I., Vilmer, N., 2013. The first sepserver event catalogue 68-MeV solar proton events observed at 1 au in 1996–2010. J. Space Weather Space Clim. 3, A12. http://dx.doi.org/10.1051/swsc/2013030.

Vos, E., Potgieter, M., 2015. New modeling of galactic proton modulation during the minimum of solar cycle 23/24. Astrophys. J. 815, 119. http://dx.doi.org/10.1088/0004-637X/815/2/119.

Wissmann, F., Burda, O., Khurana, S., Klages, T., Langner, F., 2013. Dosimetry of secondary cosmic radiation up to an altitude of 30 km. Radiat. Prot. Dosim. 161, 299–302.

Xu, W., Marshall, R., Fang, X., Turunen, E., Kero, A., 2018. On the effects of bremsstrahlung radiation during energetic electron precipitation. Geophys. Res. Lett. 45, 1167–1176. http://dx.doi.org/10.1002/2017GL076510.

Xu, W., Marshall, R.A., Tobiska, W.K., 2021. A method for calculating atmospheric radiation produced by relativistic electron precipitation. Space Weather e2021SW002735. http://dx.doi.org/10.1029/2021SW002735.

Zong, Q., Escoubet, P., Sibeck, D., Le, G., Zhang, H., 2020. Dayside magnetosphere interactions. Am. Geophys. Union http://dx.doi.org/10.1002/9781119509592.